A Lightweight Deep Learning Approach for Lithium-ion Battery RUL Estimation

Lorenzo Longarini*, Mariorosario Prist*, Alessandro Freddi*, Andrea Monteriù*, Alessandro Rongoni*, Andrea Bonci*, Paolo Cicconi†, Geremia Pompei‡,
*Department of Information Engineering, Polytechnic University of Marche, Ancona, Italy
Email: {m.prist, a.bonci, a.freddi, a.monteriu}@staff.univpm.it, {s1110740, s1114661}@studenti.univpm.it
†Dept. of Industrial, Electronic and Mechanical Engineering, Roma Tre University, Roma, Italy
Email: paolo.cicconi@uniroma3.it
‡Department of Computer Science, University of Pisa, Pisa, Italy
Email: geremia.pompei@di.unipi.it

***Abstract*—Lithium-ion batteries represent a pivotal component within contemporary energy storage solutions, exhibiting a diverse range of applications spanning from consumer electronics to electric vehicles and renewable energy systems. Nevertheless, the progressive degradation of these batteries, resulting in a reduction in capacity and performance, poses significant challenges in terms of system safety and reliability. In this context, the evaluation of the Remaining Useful Life (RUL) plays a central role in assessing the health of lithium-ion batteries. Ensuring precise and reliable RUL prediction is critical for the proper operation of a system. In this work, to address these challenges, a novel lightweight deep learning approach has been proposed for battery RUL estimation, by using voltage and current data. The proposed model is an approach based on the Echo State Networks (ESNs), which is compared to conventional deep learning models, such as Long Short-Term Memory (LSTM) networks, which require more complex architectures and substantial computational resources. The ESN-based model demonstrates a comparable predictive capacity, while substantially reducing training and inference times. The model was tested with the CALCE dataset, focused on data obtained during charge and discharge cycles of lithium-ions batteries. Specifically, under the test conditions of 1 C discharge, the ESN requires only 0.3 seconds for training and approximately 0.06 seconds for inference, thus offering a computational advantage over the LSTM model, which requires 384 seconds for training and approximately 0.19 seconds for inference with the same hardware.**

***Index Terms*—Remaining Useful Life, State of Health, Deep Learning, Long Short-Term Memory, Echo State Network, Predictive maintenance**

I. Introduction

Lithium-ion batteries are completely integrated into modern energy storage solutions, particularly in consumer electronics, electric vehicles (EVs), and renewable energy systems. Their widespread adoption is attributed to their high energy density, efficiency, and long operational life. However, battery degradation poses a significant challenge as it leads to a gradual decline in capacity and power output, directly affecting the performance and safety of the systems that rely on them. Various studies have investigated the primary causes of degradation, identifying critical factors such as charge-discharge cycles, operating temperature, and high discharge rates that contribute to electrochemical issues, including the growth of the Solid-Electrolyte Interface (SEI), the loss of active lithium, and increased internal resistance [1], [2]. The accurate monitoring of battery health is based on the estimation of two parameters: State of Health (SoH) and the Remaining Useful Life (RUL) [3], [4]. SoH estimation methodologies can be broadly categorized into physical-mathematical and empirical–statistical models. The Doyle–Fuller–Newman (DFN) model is a prominent example of a physical-mathematical approach, providing a detailed representation of battery dynamics through differential equations describing ion transport and intercalation reactions [5]. Although physical-mathematical models offer high accuracy, they require extensive knowledge of electrochemical properties and precise calibration, which can vary significantly between cells and operating conditions, making real-time application challenging [6]. On the other hand, empirical models that leverage historical data to update SoH estimates often exhibit greater computational efficiency dynamically. However, they may struggle with adaptability and predictive accuracy when well-structured datasets lack [7], [8]. Recent artificial intelligence (AI) advances have introduced data-driven techniques that further enhance SoH estimation capabilities. Methods including Genetic programming and Gaussian Process Regression (GPR) have demonstrated strong predictive performance by analyzing voltage, current, and temperature data from battery monitoring systems [9]. Deep Learning (DL) techniques have emerged as powerful tools for modeling complex relationships in data-driven applications. Unlike traditional Machine Learning (ML) methods that often rely on handcrafted features, DL models autonomously extract relevant patterns from raw sensor data, making them highly suitable for time–series prediction tasks [10], [11]. In battery health estimation, these models demonstrate superior adaptability to varying operational conditions, enabling more accurate and generalized predictions than conventional approaches. Recurrent neural networks (RNNs), particularly Long Short–Term Memory (LSTM) networks [12] and Gated Recurrent Units (GRUs) [13], have been widely explored for SoH and RUL estimation due to their ability to capture long–term dependencies in sequential data [14]. LSTMs mitigate the vanishing gradient problem typical of standard

RNNs, capturing complex degradation patterns in lithium-ion batteries. Similarly, GRUs offer a computationally efficient alternative to LSTMs by simplifying gating mechanisms while maintaining comparable predictive accuracy. Moreover, their reliance on a gradient-based optimization makes them susceptible to convergence issues, mainly when dealing with sparse or noisy data. To address these limitations, Echo State Networks (ESNs) [15] have gained increasing attention as an alternative recurrent architecture offering remarkable computational efficiency and rapid training. ESNs adopt a sparsely connected, randomly initialized reservoir that transforms input signals into a high–dimensional representation, enabling efficient learning with minimal computational overhead. Unlike LSTMs or other types of RNNs, ESNs require only training of the output layer, significantly reducing training time while maintaining strong predictive performance. The contributions of the proposed solution can be summarized as follows:

- *Proposed Strategy*: A lightweight ESN-Based approach for computationally efficient RUL estimation. This near-instantaneous feedback loop, supported by the proposed approach, enables prompt corrective measures, minimizing the likelihood of extended downtime and ensuring continuous utilization of the devices that rely on it.
- *Results evaluations*: An intensive comparative analysis of ESN performance against the LSTM benchmark has been conducted, assessing not only prediction capability but also computational efficiency.
- *Different test scenarios*: Comprehensive evaluation across different battery discharge conditions, emphasizing real–world operational versatility.

The remainder of the paper is structured as follows. Section II details the dataset, data preprocessing techniques, and the methodologies used. Section III presents experimental results and comparative analysis. Finally, Section IV summarizes the key findings, and future work.

II. Materials and Methods

This section provides a detailed overview of the proposed lightweight ESN-based approach designed for computationally efficient RUL estimation, while also introducing the LSTM-based model as a benchmark. In addition, it describes the data pre-processing methodology, the indicators used to evaluate the battery's SoH, and the validation approach.

A. Dataset

To validate the model, the CALCE dataset from the Center for Advanced Life Cycle Engineering at the University of Maryland has been utilized, which provides detailed experimental data on the behavior of lithium-ion cells [16]. Specifically, among the available lithium battery sets, the *CS2* series cells have been chosen for the proposed analysis. The datasets used are CS2_33, CS2_34, CS2_35, CS2_36, CS2_37 and CS2_38, which contain the features described in Table I. They have nominal capacity of 1100 mAh and use a $LiCoO_2$ cathode. Each cell has been tested using a CC-CV (Constant Current – Constant Voltage) protocol with an initial charge rate of 0.5C until reaching 4.2V, then the voltage is kept constant at 4.2V until the current drops below 0.05A. Similarly, the discharge is conducted up to a cut-off voltage of 2.7V.

TABLE I
Main columns of the *Channel* sheet in the CALCE dataset.

Data	Description
Data_Point	Incremental index of the sample
Test_Time (s)	Total time from the start of the test
Step_Time (s)	Duration of the current phase
Step_Index	Index that identifies the cycle phase
Cycle_Index	Index that identifies the cycle number
Current (A)	Instantaneous current value
Voltage (V)	Instantaneous voltage value
Charge_Capacity (Ah)	Accumulated charge capacity
Discharge_Capacity (Ah)	Delivered discharge capacity

B. Data Preprocessing

The process applied to the CALCE dataset has been designed to extract and preprocess the relevant features for estimating the SoH and predicting the RUL of the batteries. The dataset contains a field, *Step_Index*, that distinguishes operational phases, with a value of 2 for constant current charging, 4 for constant voltage charging, and 7 for discharge. Capacity values have been extracted from *Charge_CapacityAh* for *Step_Index* 2 and 4 and from *Discharge_CapacityAh* for *Step_Index* 7. For each file, the values of *CurrentA*, *VoltageV*, and the corresponding capacity have been extracted to create separate dataframes for charge and discharge data. The dataset, initially affected by numerous outliers, has been filtered by eliminating records with negative time values and the current peak observed during the transition from constant current to constant voltage charging. The SoH has been computed by comparing the measured capacity with the nominal capacity (1100 mAh). Input sequences have been generated via a sliding window approach that employs a historical window of 10 cycles, with an offset that can vary from 1 to 20 cycles depending on the forecast horizon of interest. Training data have been normalized by computing the mean and standard deviation of the sequences and then split into training and test sets using an $80/20$ hold-out approach.

C. State of Health Indicators

The SoH is a key metric that indicates how much of the original capacity a battery does still retain. It is described by the following equation:

$$\mathrm{SoH} = \frac{C_\mathrm{P}}{C_\mathrm{N}} \times 100 \tag{1}$$

where C_P represents the capacity actually delivered (or absorbed) in each cycle and C_N corresponds to the declared nominal capacity (in this case set to 1100mAh). In order to evaluate the SoH of the batteries represented by the CALCE datasets, the current capacity has been evaluated during either the charge or discharge phases. This enabled a comparison of the battery health status, as illustrated in Figure 1. In order to achieve accurate SoH estimates, Health Indicators (HIs) based

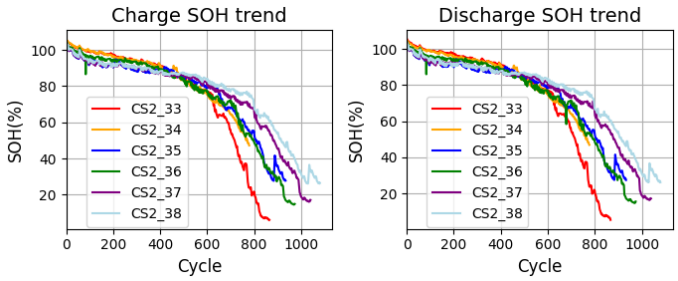

Fig. 1. SoH trend during charging and discharging for each dataset considered.

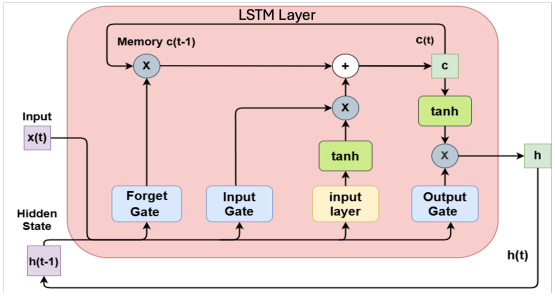

Fig. 3. LSTM architecture schema.

on the integrated measurements of voltage (HI_v) and current (HI_i) during the charging phases have been employed. The integral of the voltage over time HI_v, expressed in Volts/hour, is obtained by considering the t_0 and t_1 instants in which the voltage has a value between 3.8 V and 4.2 V, respectively:

$$\mathrm{HI}_v = \int_{t_0}^{t_1} v(t)\, dtx \tag{2}$$

Specifically, HI_v provides a reliable quantification of the energy transferred during the charging cycle, offering valuable information to monitor degradation and estimate the RUL. The trend of HI_v for the considered datasets is illustrated in Figure 2. Moreover, HI_i is the integral of the current over time, expressed in Ampere/hour, and is defined as follows:

$$\mathrm{HI}_i = \int_{t_0}^{t_1} i(t)\, dt \tag{3}$$

HI_i, is more sensitive to noise and does not show a clear trend, making it less reliable as an indicator for predictive analysis. In summary, it can be deduced that the SoH is indicative of the residual capacity of the battery. Therefore, a correlation between these variables is necessary to achieve a consistent evaluation of the degradation processes. Consequently, because HI_v measured during the charging phase offers a direct indication of the accumulated energy, it was adopted as an input feature for the model, and performance evaluation was carried out in terms of SoH.

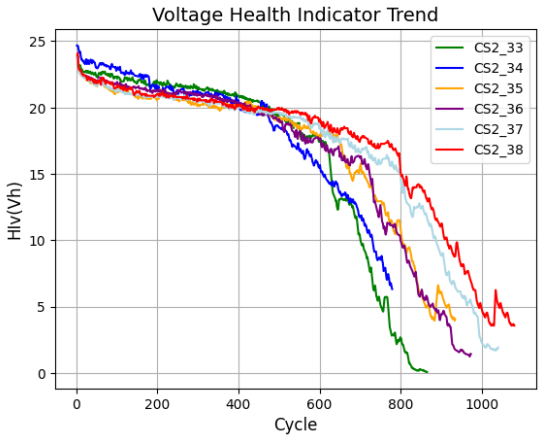

Fig. 2. Voltage Health Indicator trend across datasets.

D. Remaining Useful Life

The RUL of a battery is defined as the number of operating cycles remaining before the battery reaches its EOL stage. In this study, the battery is deemed to have reached EOL once its SoH falls below 80% of its nominal capacity. The RUL is calculated using the following equation:

$$RUL = N_{crit} - N_{act} \tag{4}$$

where N_{crit} is the cycle at which the predicted SoH falls below 80% and N_{act} is the current (or actual) cycle at the time of prediction. Instead, the percentage errors in RUL prediction have been calculated as the absolute difference between the actual and predicted critical cycle (denoted with the hat $\hat{}$ symbol), normalized with respect to the actual value:

$$\text{Error} = \frac{\left|N_{crit} - \hat{N}_{crit}\right|}{RUL} \times 100\% \tag{5}$$

E. Deep Learning Models

After identifying the data to be utilized to obtain a more accurate and robust estimation of the SoH, the subsequent experimental phase was initiated using RNN models.

1) Long Short-Term Memory: LSTM model is widely acknowledged as a significant advancement over standard RNN, as it incorporates the concept of long-term memory (See Figure 3). To consolidate existing state-of-the-art results, a series of experiments have been conducted. These experiments involved the evaluation of different hyperparameters of the LSTM model. The objective of these experiments has been to maximize the performance of the model itself. In particular, a single layer LSTM architecture consisting of 128 units, employing a ReLU activation function, the Adam optimizer, a learning rate of $5 \times 10^{-}5$, and a batch size of 64, has been determined to produce optimal predictive performance.

2) Echo State Network: The ESN is based on the Reservoir Computing paradigm, in which the recurrent component, termed ”reservoir”, is constituted by a network of randomly connected neurons. In this approach, the internal weights of the reservoir remain fixed and are not updated during training,

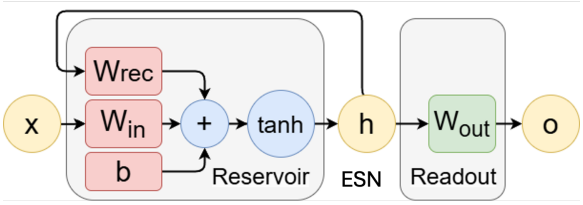

Fig. 4. ESN architecture schema.

while learning is performed exclusively at the readout level which maps the reservoir state to the desired output via a ridge regression (See Figure 4). Consequently, the ESN model is recognized for its reduced training complexity. During the course of the experiments, a number of hyperparameters have been explored via grid-search, including reservoir size, spectral radius, leaking rate, and the Ridge regularization term. Optimal results have been achieved with a reservoir of size 200, a spectral radius of 0.9, a regularization of 1×10^{-5} and a leaking rate of 0.5 (See Table II).

F. Metrics

In order to evaluate the performance of the proposed models, the following predictive and computational accuracy metrics have been used:

- Mean Absolute Error (MAE): is defined as the arithmetic mean of the absolute deviations between the observed values (y_i) and the estimated values ($\hat{y}_i$).
- Root mean square error (RMSE): useful for emphasising the largest errors.
- Training and inference times: this is employed to assess the computational complexity of the models.

III. Results

This section presents the results of the LSTM and ESN models for estimating the SoH of lithium batteries. In addition to the overall analysis, a further evaluation has been performed focusing exclusively on cycles in which the SoH exceeded 80%. This threshold has been chosen as it represents the operating range where the batteries provide optimal performance and therefore a realistic representation of the most common usage conditions. Both models have been trained on datasets characterised by a discharge rate of 1 C (in particular CS2_36 and CS2_38) and tested on different datasets, both in conditions of a discharge rate equal to 1 C and in the presence of different rates (e.g. 0.5 C).

TABLE II
ESN HYPERPARAMS GRID SEARCH.

Reservoir size	Spectral Radius	MAE (%)	RMSE (%)
50	0.9	0.8150	1.0948
50	1	0.8229	1.1140
100	0.9	0.8121	1.0904
100	1	0.8078	1.0991
200	**0.9**	**0.7884**	**1.0974**
200	1	0.7927	1.0888

TABLE III
LSTM PERFORMANCE ON VALIDATION DATASETS.

Dataset	C-Rate	MAE (%)	RMSE (%)
Dataset 33	0.5C	1.4739	1.8759
Dataset 35	1C	0.7407	0.8926
Dataset 37	1C	**0.5432**	**0.68817**

TABLE IV
EXPERIMENTAL RESULTS FOR LSTM.

SoH	Dataset	C-rate	MAE (%)	RMSE (%)
Total	Dataset 33	0.5C	1.4462	1.9416
	Dataset 35	1C	0.7764	0.9493
	Dataset 37	1C	**0.4877**	**0.6163**
$> 80\%$	Dataset 33	0.5C	1.4462	1.9416
	Dataset 35	1C	0.7764	0.9493
	Dataset 37	1C	**0.4877**	**0.6163**

A. LSTM

Following the identification of the optimal hyperparameters, the model has been subjected to further training for a total of 15.000 epochs, as recommended in the existing literature. The results are displayed in Table III. MAE and RMSE error values have been consistently found to be less than 1 percentage point when the test conditions replicate the training conditions. However, the implementation of an alternative discharge rate (e.g. 0.5 C), not foreseen during the training phase, results in a marginal increase in error, although the results remain acceptable. Given the substantial number of epochs utilised without a discernible enhancement in performance, a subsequent experiment has been undertaken with the incorporation of an Early Stopping function (with a patience parameter set to 100 epochs), allowing the stop of training after attaining a plateau. The experiment demonstrated that only 915 epochs are sufficient to achieve performances analogous to those achieved with the complete training, thus significantly reducing the computation times (up to 6 minutes and 24 seconds). In Table IV the results obtained with the classical approach and those relating to cycles with SoH higher than 80% are compared. The analysis of cycles with $SoH > 80\%$ confirm the robustness of the model, with the performance metrics remaining constant.

B. ESN

The ESN achieved comparable results in terms of accuracy while offering the advantage of a substantially reduced training time of merely 0.3 seconds. The results obtained, which include both standard performance metrics and those associated

TABLE V
EXPERIMENT RESULTS WITH THE BEST HYPERPARAMETERS FOR ESN.

SoH	Dataset	C-rate	MAE (%)	RMSE (%)
Total	Dataset 33	0.5C	1.5102	1.8943
	Dataset 35	1C	0.7527	0.9318
	Dataset 37	1C	**0.5172**	**0.6387**
$> 80\%$	Dataset 33	0.5C	1.2811	1.5815
	Dataset 35	1C	0.7538	0.9065
	Dataset 37	1C	**0.4525**	**0.6050**

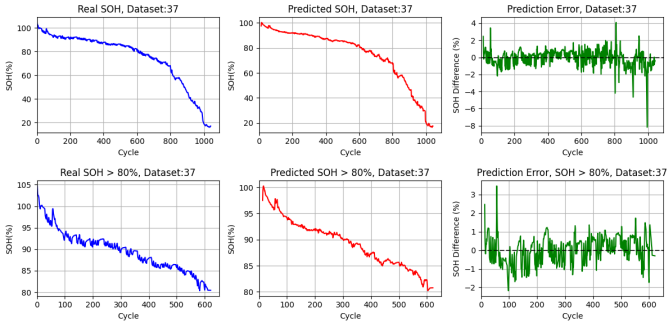

Fig. 5. SoH prediction results using ESN on dataset 37.

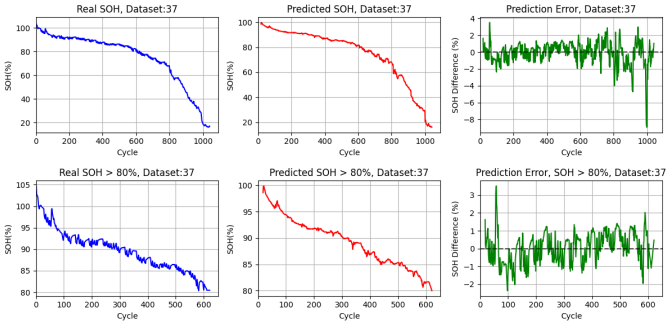

Fig. 6. SoH prediction for future 5-cycle horizons.

TABLE VI
COMPARISON OF LSTM AND ESN: TRAINING AND INFERENCE TIMES.

Model	Training Time (s)	Dataset	Inference Time (s)
LSTM	384.2	Dataset 33	0.21
		Dataset 35	0.16
		Dataset 37	0.21
		Mean	0.19
ESN	**0.3**	Dataset 33	0.057
		Dataset 35	0.057
		Dataset 37	0.068
		Mean	**0.061**

to cycles with $SoH > 80\%$, are presented in Table V and those for dataset 37 are shown in Fig. 5.

C. Comparison between LSTM and ESN

As demonstrated in Table VI, the average training and inference times obtained by the two models are summarised. It is evident that the ESN, while ensuring accuracy comparable to that of the LSTM, offers considerably reduced training and inference times. This makes the ESN a particularly important option for real-time applications, where the swiftness of the predictive process is paramount.

D. Experiments on successive cycles

In order to evaluate the model's ability to anticipate the battery degradation trend over extended time horizons, analyses have been conducted to forecast not only the immediate cycle, but also 5, 10 and 20 cycles ahead. This extension of the forecast horizon is strategic for preventive maintenance interventions and for optimal management of energy resources, as it allows to capture of the progression of deterioration. The results presented in Table VII (and Fig. 6 for dataset 37) demonstrate a modest increase in the error margin when compared to the immediate cycle forecast. This increase is anticipated, given the moderately lengthened timeframe, yet the MAE and RMSE values remain minimal, particularly for dataset 37 in 1C conditions. In the case of the 10-cycle forecast, as reported in Table VIII (and Fig. 7 for dataset 37) a further increase in errors (MAE and RMSE) is observed compared to the 5-cycle forecast. This increase in errors can be attributed to the inherent complexity and uncertainty that characterises long-term forecasting. However, the model maintains competitive performances, particularly in the case of dataset 37, highlighting its capacity to capture degradation trends over an intermediate timeframe. This finding is of particular relavance to operational planning, as it facilitates the estimation of SoH in the near future with a reasonable degree of reliability. Finally, for a 20-cycle forecast horizon (see Table IX and Fig. 8), an additional increase in errors is observed, due to the greater uncertainty associated with the long-term forecast. Despite this, the MAE and RMSE values remain acceptable, particularly in instances where the evaluation is

TABLE VII
FORECAST RESULTS FOR THE NEXT 5 CYCLES.

SoH	Dataset	C-rate	MAE (%)	RMSE (%)
Total	Dataset 33	0.5C	1.6235	2.3718
	Dataset 35	1C	1.3493	2.0029
	Dataset 37	1C	**1.0124**	**1.4616**
$> 80\%$	Dataset 33	0.5C	1.0341	1.2664
	Dataset 35	1C	1.0843	1.3377
	Dataset 37	1C	**0.7723**	**0.9382**

TABLE VIII
FORECAST RESULTS FOR THE NEXT 10 CYCLES.

SoH	Dataset	C-Rate	MAE (%)	RMSE (%)
Total	Dataset 33	0.5C	1.9546	2.7818
	Dataset 35	1C	1.7537	2.6044
	Dataset 37	1C	**1.3341**	**1.9593**
$> 80\%$	Dataset 33	0.5C	1.1999	1.4444
	Dataset 35	1C	1.2361	1.5136
	Dataset 37	1C	**0.8733**	**1.0622**

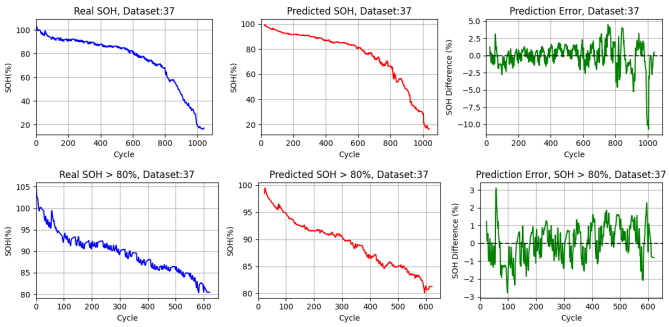

Fig. 7. SoH prediction for future 10-cycle horizons.

TABLE IX
FORECAST RESULTS FOR THE NEXT 20 CYCLES.

SoH	Dataset	C-Rate	MAE (%)	RMSE (%)
Total	Dataset 33	0.5C	2.5645	3.7763
	Dataset 35	1C	2.3103	3.4685
	Dataset 37	1C	**1.7442**	**2.7211**
$> 80\%$	Dataset 33	0.5C	1.4313	1.7324
	Dataset 35	1C	1.3671	1.6705
	Dataset 37	1C	**0.9172**	**1.1375**

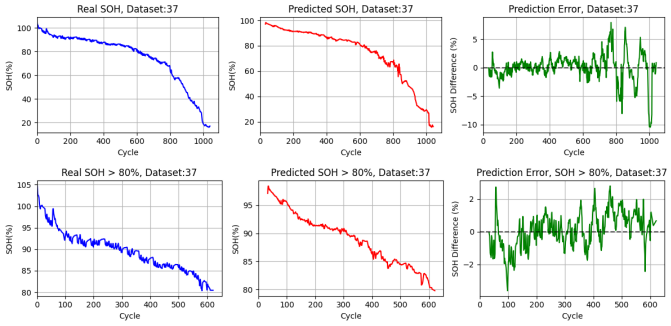

Fig. 8. SoH prediction for future 20-cycle horizons.

performed on cycles with SoH greater than 80%. This outcome indicates that, despite the model's loss of precision as the horizon lengthens, it retains a valuable predictive capacity in the battery's early stages, when degradation is less pronounced and forecasts are paramount for proactive maintenance. As illustrated in Table X, for each of the three datasets (33, 35 and 37), the percentage errors in the RUL prediction are reported, in relation to 5, 10 and 20 cycle forecasts. The RUL is defined as the difference between the critical cycle and the current forecast cycle. The reported values highlight a strong agreement between the forecasts and the observed data, thereby confirming the model's accuracy in determining the point at which the SoH drops below 80%.

IV. CONCLUSION

In this work, an innovative and lightweight approach based on a deep learning model has been proposed for the estimation of the RUL of lithium-ion batteries. This approach uses only elementary voltage and current data extracted from the CALCE dataset. The proposed model, which is based on an ESN architecture, has been designed to overcome the limitations imposed by traditional models, such as LSTM networks. Although LSTM networks offer high predictive accuracy, they require complex structures and significant computational resources. Experimental findings have shown that the ESN model achieves predictive accuracies, in terms of mean absolute error and squared error, that are comparable to those of LSTMs. However, the distinctive feature of the ESN lies in the substantial reduction in training and inference times, an element that enhances its suitability for real-time applications and for contexts in which computational efficiency is an essential requirement. Future research could involve integrating the ESN model into a distributed learning framework, such as federated learning, to facilitate decentralised and secure data management, as well as the development of continuous learning and online updating techniques to enhance the model's capacity to adapt to dynamic scenarios and real-time data.

TABLE X
PERCENTAGE ERROR IN RUL PREDICTION

Dataset	Error 5 cycles(%)	Error 10 cycles(%)	Error 20 cycles (%)
33	1.08	2.17	2.17
35	1.19	3.41	3.24
37	0.50	1.98	0.33

REFERENCES

[1] J. Zhu, Y. Wang, Y. Huang, R. B. Gopaluni, Y. Cao, M. Heere, M. J. Mühlbauer, L. Mereacre, H. Dai, X. Liu, A. Senyshyn, X. Wei, M. Knapp, and H. Ehrenberg, "Data-driven capacity estimation of commercial lithium-ion batteries from voltage relaxation," *Nature Communications*, 2022.

[2] M. Elmahallawy, T. Elfouly, A. Alouani, and A. Massoud, "A comprehensive review of lithium-ion batteries modeling, and state of health and remaining useful lifetime prediction," *IEEE Access*, 2022.

[3] B. Jia, Y. Guan, and L. Wu, "A state of health estimation framework for lithium-ion batteries using transfer components analysis," *Energies*, 2019.

[4] Y. Jiang, J. Zhang, L. Xia, and Y. Liu, "State of health estimation for lithium-ion battery using empirical degradation and error compensation models," *IEEE Access*, 2020.

[5] M. Doyle, T. F. Fuller, and J. Newman, "Modeling of galvanostatic charge and discharge of the lithium/polymer/insertion cell," *Journal of The Electrochemical Society*, vol. 140, no. 6, p. 1526, jun 1993.

[6] Z. Wang, G. Feng, X. Sun, D. Zhen, F. Gu, and A. D. Ball, "Feature extraction from charging profiles for state of health estimation of lithium-ion battery," *Journal of Physics Conference Series*, 2022.

[7] B. Zou, H. Wang, T. Zhang, M. Xiong, C. M. Xiong, Q. Sun, W. Wang, L. Zhang, C. Zhang, and H. Ruan, "A deep learning approach for state-of-health estimation of lithium-ion batteries based on differential thermal voltammetry and attention mechanism," *Frontiers in Energy Research*, 2023.

[8] C. M. Tan, P. Singh, and C. Chen, "Accurate real time on-line estimation of state-of-health and remaining useful life of li-ion batteries," *Applied Sciences*, 2020.

[9] H. Yao, X. Jia, Q. Zhao, Z. Cheng, and B. Guo, "Novel lithium-ion battery state-of-health estimation method using a genetic programming model," *IEEE Access*, 2020.

[10] Z. Huang, F. Yang, F. Xu, X. Song, and K. Tsui, "Convolutional gated recurrent unit–recurrent neural network for state-of-charge estimation of lithium-ion batteries," *IEEE Access*, vol. 7, pp. 93 139–93 149, 2019.

[11] A. Tian, Z. Chen, Z. Pan, C. Yang, Y. Wang, K. Dong, Y. Gao, and J. Jiang, "Li-ion battery state of health estimation based on short random charging segment and improved long short-term memory," *IET Signal Processing*, 2023.

[12] S. Wang, P. Takyi-Aninakwa, S. Jin, C. Yu, C. Fernández, and D.-I. Stroe, "An improved feedforward-long short-term memory modeling method for the whole-life-cycle state of charge prediction of lithium-ion batteries considering current-voltage-temperature variation," *Energy*, 2022.

[13] J. Chung, C. Gulcehre, K. Cho, and Y. Bengio, "Empirical evaluation of gated recurrent neural networks on sequence modeling," in *Advances in Neural Information Processing Systems*, 2014, pp. 1728–1736.

[14] K. Liu, L. Kang, and D. Xie, "Online state of health estimation of lithium-ion batteries based on charging process and long short-term memory recurrent neural network," *Batteries*, vol. 9, no. 2, 2023.

[15] H. Jaeger and H. Haas, "Harnessing nonlinearity: Predicting chaotic systems and saving energy in wireless communication," *science*, vol. 304, no. 5667, pp. 78–80, 2004.

[16] C. for Advanced Life Cycle Engineering (CALCE), "Calce battery data," https://calce.umd.edu/battery-data, accessed: 2025-03-14.